Applied Physics A (2018) 124:93
https://doi.org/10.1007/s00339-017-1548-3

Applied Physics A
Materials Science & Processing

Nonlinear optical response of embedded-semiconductor quantum dots covered by plasmonic metasurfaces

Masanobu Iwanaga[1] · Takaaki Mano[1] · Naoki Ikeda[1]

Received: 14 August 2017 / Accepted: 29 December 2017 / Published online: 9 January 2018

Abstract
We report the first experimental finding of nonlinear responses of photoluminescence (PL) intensity in coupling systems of plasmonic metasurface and InAs quantum dots (QDs) embedded in a GaAs substrate. We numerically designed the coupling systems and experimentally studied the PL at room temperature (RT). We found that even weak excitation induces superlinear response of the PL intensities. For comparison, we fabricated and tested a series of metallic grating couplers on the QD-embedded GaAs substrate. Although the excitation light efficiently couples to grating structures, we found that the degree of nonlinearity of the PL assisted by the plasmonic metasurfaces is higher than the case of the grating structures. These results indicate that the coupled systems of QD emitters and the plasmonic metasurfaces are essentially nonlinear systems.

Keywords Metasurface · Plasmon · Quantum dot · III–V semiconductor · Photoluminescence · Nonlinear response

1 Introduction

Plasmonic resonances have been expected to achieve significant enhancement effects for various materials for a few decades. To date, the most prominent success has been limited to a small number of cases such as enhancements for fluorescence and Raman scattering from molecules that are properly placed on the surface of plasmonic structures [1–8].

As for coupled systems of plasmonic structures and semiconductors, one of the most widely known results is plasmonic nanolasers [9–11]. The basic design concept is to employ plasmon-assisted waveguides with optical gain. Thus, although the plasmons do contribute to the lasing, the role of plasmons is secondary, meaning that the stimulated emissions can be induced in the gain waveguides without the use of plasmonic resonances. Another unconventional role of plasmons reported to date is hot-electron generation [12]. Plasmons are usually understood in the classical sense; however, the hot electrons strongly suggest that electrons in nanostructured metals can be ejected at the plasmonic resonances, being considered as a non-classical effect associated with plasmonic resonances. Thus, although the metallic-nanostructure-based plasmonic effects involving semiconductors are intriguing, the corresponding studies have been limited to a very small number of works.

Here, we report a series of experiments for a basic configuration that comprises a QD-grown semiconductor and plasmonic structures fabricated on the semiconductor surface. Specifically, a III–V semiconductor based on a GaAs substrate is used, and single-layer plasmonic structures are incorporated, being expected to assist PL emission from the QDs out of the substrate into free space.

Figure 1a shows a schematic of Au-mesh plasmonic metasurface on a GaAs substrate; the metasurface consists of a square array of apertures of a square shape, with the Au thickness of 35 nm and Au-mesh width of 3/11 of the mesh period. Figure 1b shows numerically calculated reflectance (R) spectra for three different periods $a = 270$, 300, and 330 nm, displayed with the light blue, blue, and light purple lines, respectively. The R dips represent plasmonic resonances, which are found to be tunable in the near-infrared spectral range; therefore, we used this mesh-type metasurface in this study. Figure 1b also shows a computed R spectrum of a flat GaAs substrate of 400 µm thickness (black line).

Figure 1c illustrates a line-and-space (LS)-type grating on a GaAs substrate; the LS-type grating is designed to have a LS ratio of 5:6 and Au thickness of 100 nm for better coupling with the illumination light. Figure 1d shows R spectra

✉ Masanobu Iwanaga
iwanaga.masanobu@nims.go.jp

[1] National Institute for Materials Science (NIMS), 1-1 Namiki, Tsukuba 305-0044, Japan

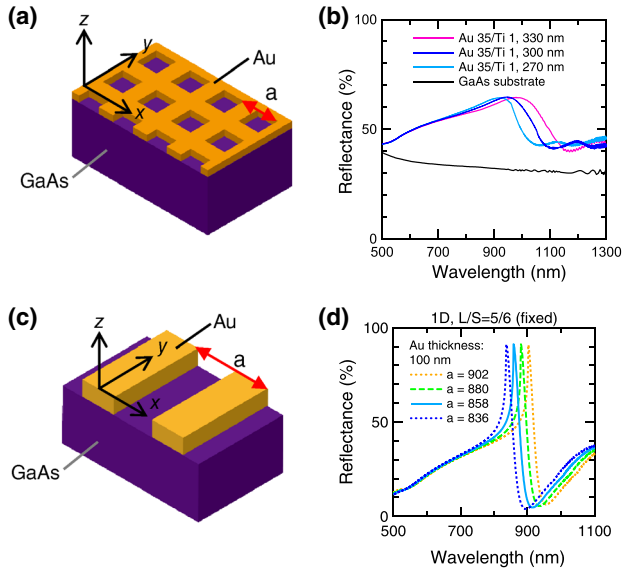

Fig. 1 **a** Schematic of a Au-mesh plasmonic metasurface, which consists of a square array of apertures and is designed to have a resonance in the near-infrared range. **b** Numerically calculated R spectra of the plasmonic metasurfaces with periods of 270 (light blue), 300 (blue), and 330 nm (light purple). The calculated R spectrum of a bulk GaAs substrate (black) is also shown. **c** Schematic of a LS-type grating coupler on a GaAs substrate. **d** Numerically calculated R spectra of LS-type gratings on GaAs substrates. The spectra for periods of $a = 836$, 858, 880, and 902 nm are shown with the dotted blue, solid light blue, dotted green, and dotted yellow lines, respectively

numerically calculated for periods $a = 836$, 858, 880, and 902 nm, corresponding to the dotted blue, solid light blue, dotted green, and dotted yellow lines, respectively.

2 Numerical and experimental methods

2.1 Numerical implementation

The plasmonic metasurfaces and LS gratings were numerically designed using the rigorous coupled-wave analysis (RCWA) method [13], which is a method to numerically solve Maxwell's equations in arbitrary periodic systems and is suitable to evaluate their linear optical spectra such as reflection and transmission. We further combine the RCWA method with a scattering matrix algorithm [14], to handle stacked structures of interest. The numerical implementations were executed on supercomputers in a multi-parallel manner.

For realistic computations, we adopted material parameters such as the complex permittivities of the constituent materials from the literature [15] and a database [16], and used a representative value for air of 1.00054. We note that, in the computations, the GaAs substrates with embedded InAs QDs were simply approximated as GaAs substrates. This approximation was valid for the present purpose of designing plasmonic structures with the resonances around the PL wavelengths.

2.2 Growth of InAs QDs

The sample was grown on a n^+-GaAs (100) substrate using a standard solid-source molecular beam epitaxy system. The layered structure was grown on the n^+-GaAs substrate in the following order: (1) a 500 nm GaAs buffer, (2) 50 nm of $Al_{0.3}Ga_{0.7}As$, (3) 50 nm of GaAs, (4) InAs QDs of approximately 1.7 monolayers (MLs), (5) 20 nm of GaAs, (6) 20 nm of $Al_{0.3}Ga_{0.7}As$, and (7) a 10 nm GaAs capping layer. For the formation of InAs QDs, 2 MLs of InAs (rate 0.005 ML/s) were supplied at 500 °C.

The AlGaAs layers were introduced as barrier layers for the InAs-QD layer. The density of the grown InAs QDs was estimated to be approximately $3 \times 10\,\mu m^{-2}$ from atomic force microscopy images (not shown here).

2.3 Nanofabrication procedures

The designed plasmonic metasurfaces and LS gratings were fabricated through a liftoff process as follows.

1. The designed nanopatterns were written in a positive-type resist on the GaAs substrate with electron-beam (EB) lithography.
2. Au and Ti were normally deposited onto the nanopatterned EB resist with a 700 mm distance between the deposition sources and the samples. Note that Ti was incorporated as an adhesion layer between the Au layer and the GaAs substrates, with the thickness kept at 1 nm. The thickness of Au was 35 and 100 nm for the plasmonic metasurfaces and LS gratings, respectively.
3. The EB resist was removed in a wet process, and the designed nanopatterns were obtained. The dimensions of the resultant nanopattern tips were about $1 \times 1\,mm^2$.

2.4 Optical measurements

PL measurements were carried out at RT in an illumination-and-collection setup for μ-PL measurement [8]. Excitation light was illuminated almost normally onto the samples with a 10× objective lens with a numerical aperture of 0.26. The PL was collected with the same objective lens. The excitation light was emitted from a continuous-wave single-mode laser with an output wavelength of 532.0 nm, and the intensity was monitored using a variable neutral-density filter in the objective lens path. The collected PL was transferred through an optical fiber, spectrally resolved by a spectrometer, and detected using a charge-coupled device camera, with typical exposure times of 1 s.

The R spectra of the plasmonic metasurfaces and LS-type gratings were measured in the same setup. Incident white light was introduced into the beam path, and the reflection signals were measured at the normal incidence. The reference signal was measured using a calibrated Al mirror.

3 Results and discussion

3.1 InAs QDs covered by plasmonic metasurfaces

Figure 2 shows the measured PL and R spectra of the plasmonic-metasurface-covered GaAs substrates with embedded InAs QDs. Figure 2a shows the PL (solid line) and R (dashed line) spectra detected through the Au-mesh metasurface covering the QD-grown GaAs substrate; the period a was $a = 250$ nm. There appeared three PL peaks coming from excitons in the QDs (red arrow), higher excitons (green arrow), and excitons in the bulk GaAs (light blue arrow). The plasmonic metasurface with $a = 250$ nm has a resonance at 910 nm, corresponding to a dip in the R spectrum and tuned to the QD-exciton peak.

Figure 2b presents the PL intensities at the three peaks in Fig. 2a for the excitation intensity; the colors of the PL plots (circles and closed squares) are matched to the arrow colors in Fig. 2a. The PL data are represented in the log-log scale. As reference, we also plot scattered intensity of the excitation light (open squares); the scattered intensity is approximated by linear response, that is, $I^{1.0}$ where I denotes intensity of excitation-laser light. In contrast, the PL intensities detected through the plasmonic metasurfaces obviously deviate from the linear response; accordingly, we fit them as follows.

The PL intensities per unit time, I_{PL}, which depend linearly or nonlinearly on the excitation-laser-light intensity I on the sample surfaces, are expressed with an equation in the log-log representation such as

$$\log_{10}(I_{PL}) = \alpha \log_{10}(I) + C \quad (1)$$

where α is power index of the excitation intensity and C is constant. In Fig. 2b, the three PL-peak intensities were fitted using Eq. (1) and were found to have nonlinear power indices such that $\alpha \approx 2$. The experimental condition was not strong excitation regime but weak excitation. Therefore, the nonlinear PL response has an unusual character. Indeed, we confirmed that the GaAs substrate without the plasmonic metasurface exhibits a linear PL response under the photo-excitation condition.

Figure 2c shows a top-view scanning electron microscope (SEM) image of the sample used in the measurement for Fig. 2a, b; the white scale bar indicates 200 nm. The period was set to 250 nm and the averaged Au line width was approximately 68 nm. We also fabricated a plasmonic

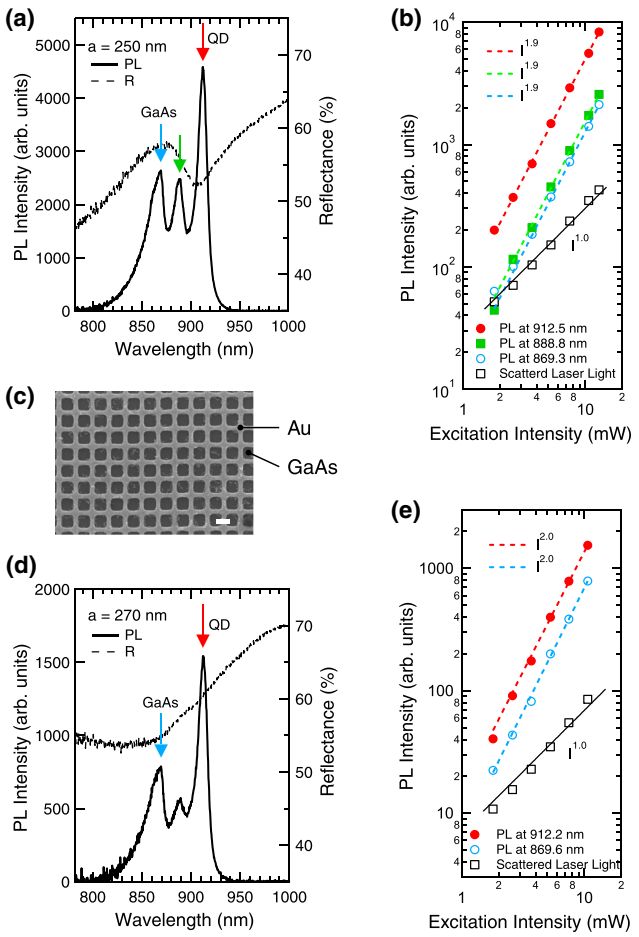

Fig. 2 **a** Measured PL (solid line) and R (dashed line) spectra for the plasmonic metasurface with $a = 250$ nm. The R spectrum is plotted for the right axis. **b** PL intensities at the three peaks in **a**, plotted as functions of the excitation intensity. Dashed lines are fits of the PL intensities using Eq. (1). The scattered laser light intensity (open square) is also plotted for reference. The PL intensities are fitted using Eq. (1). **c** Top-view SEM image of the Au-mesh metasurface with $a = 250$ nm. White scale bar indicates 200 nm. **d** PL and R spectra through the plasmonic metasurface with $a = 270$ nm. **e** PL intensities through the metasurface with $a = 270$ nm, as functions of the excitation intensity

metasurface with a period of 270 nm and an averaged Au line width of 83 nm.

Figure 2d shows the PL (solid line) and R (dashed line) spectra of a plasmonic metasurface with a period of $a = 270$ nm. The R spectrum indicates that the plasmonic resonance is not well tuned to the QD PL wavelength, indicated by a red arrow. Nevertheless, Fig. 2e shows that the PL-peak intensities exhibit nonlinear (or superlinear) responses, similarly to Fig. 2b. This is partially because the plasmonic resonance is rather broad and can also contribute at the wavelength range near the resonance.

Figure 3 shows numerically calculated electric field intensity $|\mathbf{E}|^2$ distributions for the plasmonic metasurface

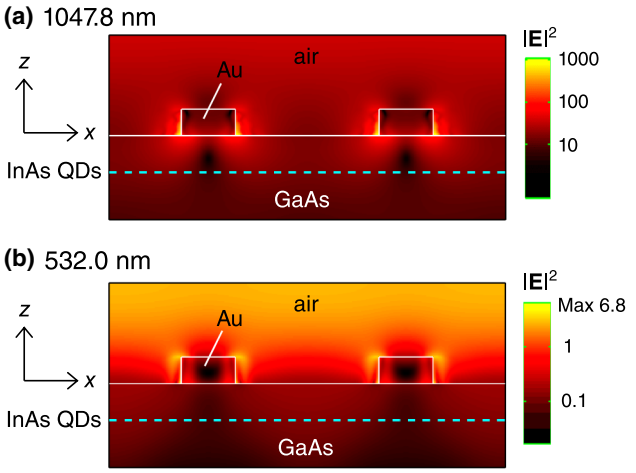

Fig. 3 Numerically calculated electric-field-intensity $|\mathbf{E}|^2$ distributions for a plasmonic metasurface with $a = 270$ nm. An xz-section view is shown, which goes through the center of the square apertures. The incident wavelengths are **a** 1047.8 nm and **b** 532.0 nm. The distributions are represented in the log scale. The depth positions of the InAs QDs are indicated by dashed water blue lines

with $a = 270$ nm; an xz-section view is presented, going through the center of square the apertures. The $|\mathbf{E}|^2$ distributions were evaluated using a method described in Sect. 2.1. The design of the plasmonic metasurface is shown in Fig. 1a. The R spectrum in Fig. 1b shows a plasmonic resonance around 1048 nm, which is seen as a R dip. Figure 3a shows the resonant $|\mathbf{E}|^2$ distribution at 1047.8 nm. Intense electric fields ($|\mathbf{E}|^2 > 100$) are localized at the sidewall of the Au mesh. The $|\mathbf{E}|^2$ distributions are shown with the log scale for better visibility. We set the incident field as $|\mathbf{E}|^2 = 1$. Thus, the resonant fields are significantly enhanced, whereas the $|\mathbf{E}|^2$ distribution at the InAs-QD embedded position (dashed water blue line) is substantially weaker than the intense fields at the Au sidewall, with estimated values of $|\mathbf{E}|^2 \sim 10$ or less. Thus, some degree of resonant enhancement is expected, whereas extremely strong electric-field enhancement for the PL-emission process is unlikely. We note that the incidence was set to come from the top in the xz plane and to be polarized in the x direction.

Figure 3b shows the $|\mathbf{E}|^2$ distribution for the excitation wavelength of 532.0 nm. Although the $|\mathbf{E}|^2$ is locally enhanced at the upper corners of the Au mesh by several times, it decays at the position of the InAs QDs (dashed water blue line) to small values of $|\mathbf{E}|^2 \sim 0.2$. In fact, there is no prominent plasmonic resonance at 532.0 nm, as shown in Fig. 1b. Therefore, electric-field enhancement is not expected in the excitation process. Nevertheless, the observed PL response is distinct from a linear response. Thus, the results in Figs. 2 and 3 suggest that the present coupled systems of InAs QDs and plasmonic metasurfaces are nonlinear systems.

3.2 InAs QDs covered by LS grating couplers

Figure 4 shows a set of experimental results on the embedded InAs QDs and a LS-type grating coupler with a period of $a = 858$ nm, fabricated on the GaAs substrate with embedded InAs QDs.

Figure 4a shows the RT PL spectrum of the GaAs substrate with embedded InAs QDs and without any plasmonic structure. Two peaks are prominent; one appears at a shorter wavelengths around 870 nm, and the other peaks at 910 nm. The former mainly comes from free excitons in the GaAs substrate and higher-order excitons in the InAs QDs, while the latter originates from excitons in the QDs. We note that the PL spectrum has a different shape from that shown in Fig. 2, due to the non-uniform growth of the QDs on the GaAs wafer.

Figure 4b shows the dependence of the PL intensities on the excitation intensity for the two peaks in Fig. 4a. Blue closed circles denote the PL intensities of the shorter-wavelength peak, while red open squares the PL intensities of the longer-wavelength peak. The measured PL intensities at the shorter-wavelength peak were fitted using Eq. (1). Since the PL intensities exhibit different behavior for the weak excitation less than 2 mW and the stronger excitation, we fitted the data in two ways: black solid line corresponds to the weak excitation regime and black dotted line corresponds to the other regime. The fitted results indicate that the PL intensities tend to exhibit a slightly nonlinear response ($I^{1.3}$ or $I^{1.1}$) and that the nonlinearity is relatively larger in the weak excitation regime. This nonlinearity probably come in part from PL component of higher-order excitons in the QDs, which overlaps with the broad shorter-wavelength PL band at 870 nm. In contrast, the longer-wavelength PL component shows a sublinear response under excitation more than 2 mW.

Figure 4c shows the PL (red line) and R (black line) spectra of the GaAs substrate with a LS grating coupler. The period of the LS coupler was 858 nm in accordance with the numerical design in Fig. 1d. The R dip around 900 nm is tuned to the longer-wavelength PL peak.

Figure 4d shows the dependence of the PL intensities on the excitation intensity, similar display to Fig. 4b. The fitted curves using Eq. (1) reveal enhanced nonlinear (or superlinear) response of the PL intensities; the power index α in Eq. (1) is 1.6 and 1.3 in the weak excitation ($\lesssim 2$ mW) and the stronger excitation, respectively. Evidently, the power index is higher than that without the LS coupler.

Table 1 lists structural, optical, and nonlinear parameters of the LS-type grating couplers fabricated in this study. The measured results on the LS-type grating with $a = 858$ nm are shown in Fig. 4. Additionally, the averaged Au line widths

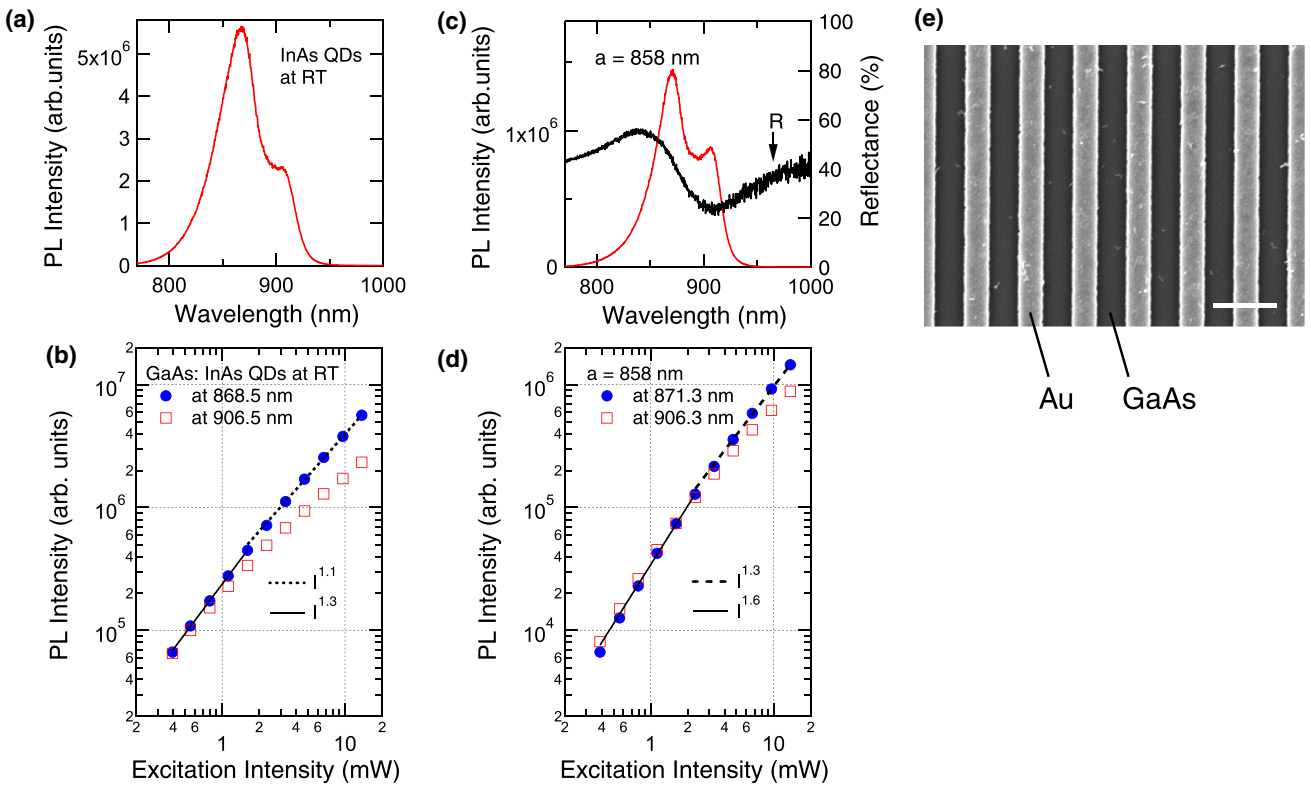

Fig. 4 **a** Measured PL spectra of InAs QDs at RT. **b** PL intensities at two peaks of 868.5 nm (blue closed circles) and 906.5 nm (red open squares) in **a**, as functions of the excitation intensity. The data is plotted in the log-log scale, being fitted with Eq. (1) (solid and dotted lines). **c** PL (red) and R (black) spectra of a LS pattern with a periodic of $a = 858$ nm on the InAs QDs. The R spectrum is plotted for the right axis. **d** PL intensities at two peaks of 871.3 nm (blue closed circles) and 906.3 nm (red open circles) in **c**, plotted in a similar way to **b**. **e** Top-view SEM image of the LS pattern with $a = 858$ nm. The white scale bar indicates 1 μm

Table 1 List of fabricated LS-type grating couplers

Period	Wavelength at the R dip	Power index α
836	896	1.5 (1.3)
858	908	1.6 (1.3)
880	932	1.6 (1.3)
902	955	1.6 (1.3)

The structural dimensions and wavelengths are shown in the units of nm. The power indices α in Eq. (1) are listed in the order from weak to relatively stronger excitation; the latter is written in parentheses. The measured data for the period of 858 nm are shown in Fig. 4

are 369, 398, 418, and 429 nm for $a = 836$, 858, 880, and 902 nm, respectively.

Figure 5 shows numerically calculated xz-section-view $|\mathbf{E}|^2$ distributions around the LS-type grating coupler with $a = 858$ nm. Figure 1c shows the corresponding design. The R spectrum is shown in Fig. 1d and exhibits an impedance-matching (i.e., low-R) resonance at 915.4 nm as the R dip. The corresponding $|\mathbf{E}|^2$ distribution is shown with the log scale in Fig. 5a, strongly localized at the top and sidewall of the Au lines; in contrast, the $|\mathbf{E}|^2$ distribution at the positions

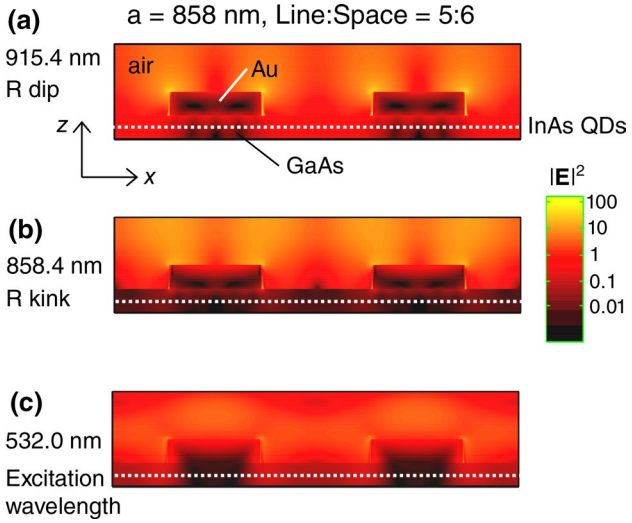

Fig. 5 $|\mathbf{E}|^2$ distributions near the LS-grating coupler with a period of $a = 858$ nm at **a** 915.4 nm, **b** 858.4 nm, and **c** 532.0 nm; the distributions correspond to the R dip in Fig. 1d, the R kink in Fig. 1d, and the excitation wavelength, respectively. The three distributions are shown with the log scale and the scale bar is commonly shown on the right-hand side. The positions of the InAs QDs are indicated by white dotted lines

of the InAs QDs (white dotted line) is not enhanced relatively to the incident $|\mathbf{E}|^2$, which is unity. The scale bar for all the data in Fig. 5 is shown on the right-hand side. Incidence was set similarly to that in Fig. 3.

Figure 5b shows the $|\mathbf{E}|^2$ distribution at the R kink of 858.4 nm in Fig. 1d. The wavelength is very close to the period and associated with the diffractive effect that can be seen as periodic patterns in the air domain. We note that the $|\mathbf{E}|^2$ takes small values (< 0.1) at the positions of the InAs QDs and is not enhanced.

Figure 5c shows the $|\mathbf{E}|^2$ distribution at the excitation wavelength of 532.0 nm, where there is hardly a spectral feature as shown in Fig. 1d. Although the Au lines work as light absorbers, the field distribution hardly contributes to the efficient excitation of the InAs QDs.

Let us shortly summarize the results for the LS grating couplers. We clarified that, in Fig. 4, the nonlinear power indices increase in the LS-coupler-loaded configurations in comparison with those for the GaAs substrate without the LS coupler. The $|\mathbf{E}|^2$ distributions in Fig. 5 suggest that, although the LS-type gratings are efficient light absorbers, they are not so suitable as plasmon-enhancing structures. Nevertheless, we point out that, unexpectedly, the LS-type plasmonic couplers have an effect to increase the nonlinearity of the coupled systems.

3.3 Nonlinear PL-emission process

Here, we briefly sum up the experimental results shown so far and discuss the observed nonlinear PL emission.

The experimental results show that, when plasmonic structures are incorporated, the PL response of the QDs to the excitation intensity becomes nonlinear; quantitatively, the power index α in Eq. (1) is clearly larger than 1.0. In particular, for the Au-mesh plasmonic metasurfaces fabricated on the GaAs substrate, the power index is large (i.e., $\alpha \approx 2$) under the weak excitation. These results indicate unconventional PL response, which is not expected in the conventional semiconductor physics.

Furthermore, we compared the two plasmonic structures fabricated on the GaAs substrates, namely, the Au-mesh plasmonic metasurfaces and the LS-type grating couplers. As light absorbers, the LS couplers are superior to the plasmonic metasurfaces. However, based on the values of the power index α, the plasmonic metasurfaces enable larger nonlinear PL response. This result was examined from the viewpoint of the resonant electric-field intensities $|\mathbf{E}|^2$. We found that the plasmonic metasurfaces exhibit larger values of $|\mathbf{E}|^2$ at the positions of the InAs QDs. Thus, the qualitative tendency of the nonlinearity can be understood.

However, the $|\mathbf{E}|^2$ distributions were evaluated in the classical framework and cannot fully describe the nonlinearity since the purely classical description results in linear responses under weak excitation. Therefore, a theoretical model should be developed that would be able to describe the nonlinear response. It seems possible that hot electrons generated in the plasmonic structures could contribute to multiple excitation in the QDs. To our knowledge, such a model for configurations similar to the one investigated here has not been developed.

4 Conclusions

We experimentally demonstrated nonlinear (or superlinear) response from coupled systems of III–V semiconductor QDs and plasmonic structures. In particular, it was clarified that the coupled systems are nonlinear even under weak excitation. Furthermore, we showed that the nonlinearity is quantitatively larger for the Au-mesh plasmonic metasurfaces than for the LS grating couplers. These experimental findings strongly suggest that unconventional interplay takes place in the coupled system of the QDs and plasmonic structures on the substrate surface.

Acknowledgements This study was partially supported by JSPS KAKENHI Grant (Number JP17H01066) from the Japan Society for Promotion of Science, by HPCI System Research Project (ID: hp170134) through Cyberscience Center, Tohoku University, and by the 4th midterm research project in NIMS. The nanofabrication was conducted at Namiki Foundry and NanoIntegrated Platform in NIMS.

References

1. J.R. Lakowicz, K. Ray, M. Chowdhury, H. Szmacinski, Y. Fu, J. Zhang, K. Nowaczyk, Analyst **133**, 1308 (2008)
2. M. Bauch, K. Toma, M. Toma, Q. Zhang, J. Dostalek, Plasmonics **9**, 781 (2014)
3. M. Iwanaga, *Plasmonic Resonators: Fundamentals, Advances, and Applications* (Pan Stanford Publishing, Singapore, 2016)
4. W. Zhang, F. Ding, W.D. Li, Y. Wang, J. Hu, S.Y. Chou, Nanotechnol. **23**, 225–301 (2012)
5. L. Zhou, F. Ding, H. Chen, W. Ding, W. Zhang, S.Y. Chou, Anal. Chem. **84**, 4489 (2012)
6. M. Iwanaga, B. Choi, Nano Lett. **15**, 1904 (2015)
7. B. Choi, M. Iwanaga, H.T. Miyazaki, Y. Sugimoto, A. Ohtake, K. Sakoda, Chem. Commun. **51**, 11470 (2015)
8. M. Iwanaga, B. Choi, H.T. Miyazaki, Y. Sugimoto, Nanoscale **8**, 11099 (2016)
9. R.F. Oulton, V.J. Sorger, T. Zentgraf, R.M. Ma, C. Gladden, L. Dai, G. Bartal, X. Zhang, Nature **461**, 629 (2009)
10. M. Khajavikhan, A. Simic, M. Katz, J.H. Lee, B. Slutsky, A. Mizahi, V. Lomakin, Y. Fainman, Nature **482**, 204 (2012)
11. Y.J. Lu, J. Kim, H.Y. Chen, C. Wu, N. Dabidian, C.E. Sanders, C.Y. Wang, M.Y. Lu, B.H. Li, X. Qiu, W.H. Chang, L.J. Chen, G. Shvets, C.K. Shih, S. Gwo, Science **337**, 450 (2012)
12. M.W. Knight, H. Sobhani, P. Nordlander, N.J. Halas, Science **332**, 702 (2011)
13. L. Li, J. Opt. Soc. Am. A **14**, 2758 (1997)
14. L. Li, J. Opt. Soc. Am. A **13**, 1024 (1996)
15. A.D. Rakić, A.B. Djurišić, J.M. Elazar, M.L. Majewski, Appl. Opt. **37**, 5271 (1998)
16. http://www.ioffe.ru/SVA/NSM/nk/index.html. Accessed 9 Jan 2018